HHS Public Access

Author manuscript

Adv Healthc Mater. Author manuscript; available in PMC 2021 April 01.

Published in final edited form as:

Adv Healthc Mater. 2020 April ; 9(8): e1901214. doi:10.1002/adhm.201901214.

Relaxation of Extracellular Matrix Forces Directs Crypt Formation and Architecture in Intestinal Organoids

Ella A. Hushka,
Department of Chemical and Biological Engineering, University of Colorado Boulder, Boulder, CO 80309, USA

The BioFrontiers Institute, University of Colorado Boulder, Boulder, CO 80303, USA

F. Max Yavitt,
Department of Chemical and Biological Engineering, University of Colorado Boulder, Boulder, CO 80309, USA

The BioFrontiers Institute, University of Colorado Boulder, Boulder, CO 80303, USA

Tobin E. Brown,
Department of Chemical and Biological Engineering, University of Colorado Boulder, Boulder, CO 80309, USA

The BioFrontiers Institute, University of Colorado Boulder, Boulder, CO 80303, USA

Peter J. Dempsey,
Department of Pediatrics, University of Colorado, Denver, CO 80204, USA

Kristi S. Anseth
Department of Chemical and Biological Engineering, University of Colorado Boulder, Boulder, CO 80309, USA

The BioFrontiers Institute, University of Colorado Boulder, Boulder, CO 80303, USA

Abstract

Intestinal organoid protocols rely on the use of extracellular scaffolds, typically Matrigel, and upon switching from growth to differentiation promoting media, a symmetry breaking event takes place. During this stage, the first bud like structures analogous to crypts protrude from the central body and differentiation ensues. While organoids provide unparalleled architectural and functional complexity, this sophistication is also responsible for the high variability and lack of reproducibility of uniform crypt-villus structures. If function follows form in organoids, such structural variability carries potential limitations for translational applications (e.g., drug screening). Consequently, there is interest in developing synthetic biomaterials to direct organoid growth and differentiation. It has been hypothesized that synthetic scaffold softening is necessary for crypt development, and these mechanical requirements raise the question, what compressive

kristi.anseth@colorado.edu.
Current Address: Material Measurement Laboratory, National Institute of Standards and Technology, Boulder, CO 80305, USA

Supporting Information
Supporting Information is available from the Wiley Online Library or from the author.

forces and subsequent relaxation are necessary for organoid maturation? To that end, we employed allyl sulfide hydrogels as a synthetic extracellular matrix mimic, but with photocleavable bonds that temporally regulate the material's bulk modulus. By varying the extent of matrix softening, we demonstrate that crypt formation, size and number per colony are functions of matrix softening. An understanding of the mechanical dependence of crypt architecture is necessary to instruct homogenous, reproducible organoids for clinical applications.

Graphical Abstact

Allyl sulfide hydrogels were employed as a synthetic extracellular matrix with photocleavable bonds to temporally regulate the bulk modulus. By varying the extent of matrix softening, we demonstrate that intestinal organoid crypt formation, size and number per colony are functions of matrix softening.

Keywords

intestinal organoids; hydrogels; mechanosensing; adaptable materials; photodegradation

1. Introduction

Organoids are self-organized, three-dimensional (3D) tissues that are typically derived from stem cells grown in a matrix and capture key functional, structural, and biological complexity of the organ from which they are derived. This unparalleled biomimicry holds great promise as a means to study organogenesis and disease, screen drug candidates, personalize medicine and supply tissue for transplantation. Clevers et. al. was the first to culture intestinal organoids with a crypt-villus architecture derived from single isolated adult intestinal stem cells (ISCs).[1] Most work in the literature to date encapsulates ISCs in Matrigel, a supportive three-dimensional matrix, and in this environment single ISCs proliferate and organize into a polarized, spherical cyst of intestinal stem cells. Upon switching from growth to differentiation promoting media, a symmetry breaking event takes place, during which the first crypt protrudes from the central body and subsequent differentiation takes place into spatially restricted lineages.[2] Mature intestinal organoids show Paneth cells, a committed secretory lineage, intercalated in the crypt with ISCs. Meanwhile, other secretory and absorptive cell types, including enterocytes, goblet, tuft and enteroendocrine cells, are restricted to the villus regions.[3,4] While organoids provide an unparalleled architectural and functional complexity, this sophistication is also responsible for the high variability and lack of reproducibility of uniform crypt-villus structures. For example, in organoids grown in Matrigel, the crypt-villus architecture is largely random, and the location, number and size of crypts has yet to be controlled. If function follows form in organoids, such high structural variability carries potential limitations for translational applications such as drug screening, in which controlled and uniform organoid structures may be required for reproducible and predictable function.

As a result, there has been growing interest in the development of synthetic biomaterials and bioengineering 3D culture methods to direct organoid growth. Amongst the first of these efforts, Cruz-Acuña et al. demonstrated that 4-arm poly(ethylene) (PEG) maleimide based

hydrogels supported human intestinal organoid viability, development and differentiation.[5] Gjorevski et al. used hydrolytically softening, hybrid hydrogels that were formed from two, 8-arm PEG-peptide conjugates (*n-PEG-MMP* and *n-PEG-Gln*) using factor XIIIa to crosslink. With this 3D material, they demonstrated that intestinal organoids not only require a supportive 3D matrix with a defined elasticity for colony formation, but that matrix softening is needed for symmetry breaking, crypt formation and differentiation.[6] They also proposed a specific modulus range that best supports colony formation and a range that best allows for crypt protrusion. While synthetic materials offer specific advantages over Matrigel (e.g., for transplantation of organoids), these material systems can still lead to high variability in crypt number and architecture, limiting the questions that can be answered with these systems. Hydrolytically controlled systems rely on pre-defined degradation kinetics that utilize stochastic cleaving events, offering limited control over degradation. To date, no methods have been developed for an organoid-hydrogel system that is highly systematic and controlled. Inspired by this work, we exploited photochemical reactions and their temporal control with an interest in learning how mechanical cues influence symmetry breaking and subsequent crypt architecture.

Toward the goal of on-demand material regulation, photodegradable materials have been used to investigate the effect of stiffness on cellular response, as they provide both spatial and temporal control.[7–13] In one recent example, Brown et al. reported on a photodegradable PEG hydrogel utilizing allyl sulfide crosslinks.[14–17] Here, photoinitiated radicals chain transfer to soluble monofunctional thiols that participate in radical mediated exchange with allyl sulfide functionalities. Upon cleavage, the allyl sulfide functionality is regenerated, along with a radical species that can initiate further exchange reactions. In this manner, a single photon can initiate multiple cleavage events, thereby amplifying degradation compared to traditional photodegradable hydrogel platforms.[18–21] As a demonstration, a one cm thick hydrogel underwent complete degradation in 60 seconds upon irradiation with 365 nm light.

Here, allyl sulfide hydrogels were optimized for the culture of intestinal organoids and the photochemical control of the material properties was used to investigate the effects of on-demand matrix softening on crypt formation and architecture. Results show that the allyl sulfide hydrogels support colony survival and that colony survival is mechanosensitive, as it depends on macromer weight and the subsequent moduli. Next, by varying the duration of irradiation, and therefore the magnitude of the softened modulus, we establish five different conditions, with each condition reaching a different final extent of degradation. Experiments were designed to probe how organoid maturation in the form of crypt formation depends on local mechanical cues. Results reveal that crypt forming efficiency, as marked by the presence of Paneth cells in budding structures, is mechanically responsive, as crypt formation improves and then declines with increasing matrix softening. Further characterization of crypt architecture shows that crypt length and number per colony are functions of matrix softening, following the same trend as crypt forming efficiency. An understanding of the influence of mechanical cues on symmetry breaking and subsequent crypt architecture is necessary to instruct homogenous, reproducible organoids for clinical applications.

2. Engineered Photodegradable Scaffolds

Allyl sulfide hydrogels with photocleavable linkers were adapted to act as an extracellular matrix mimic to support organoid growth. Crosslinked hydrogels were formed between a tetrafunctionalized PEG dibenzocyclooctyne (PEG-DBCO) and an allyl sulfide bis(azide) through a strain promoted azide alkyne cycloaddition (SPAAC) reaction (Figure 1a,b).[7,14,22,23] At physiological conditions, this bio-orthogonal reaction occurs rapidly with crosslinkers reaching the gel point (crossover of G' and G") in <30 seconds and achieving equilibrium storage modulus in < 5 min (Figure 1c).[14] By varying macromer weight percent during hydrogel formation, the final matrix crosslinking density is varied and can be further tuned to match a desired modulus. Rheological measurements of the final hydrogels containing 3 to 7 wt% PEG macromer yielded storage modulus values ranging from 340 +/− 60 to 1900 +/− 600 Pa (Figure 1d). These modulus values span the range of what has previously been demonstrated as an ideal modulus for colony growth from single intestinal stem cells.[6]

After formation, photoinduced degradation is achieved by irradiation with 365 nm light in the presence of a monofunctionalized thiol (glutathione, GSH) and a photo initiator (lithium phenyl-2,4,6-trimethylbenzoylphosphinate, LAP).[14] Allyl sulfide bis(azide) reacts with thiyl radicals from GSH to form a radical intermediate, resulting in fragmentation of crosslinks and regeneration of the thiyl radical and allyl sulfide bis(azide). The newly generated thiyl radical then undergoes chain transfer to a soluble thiol species, initiating further exchanges, thus amplifying degradation (i.e., cleaving the allyl sulfide crosslinker to a pendant functionality via reaction with GSH) (Figure 2a, S1). By controlling the duration of light exposure, the gel modulus can be precisely and temporally controlled from a reduction in the bulk modulus to complete erosion.

We can precisely manipulate the hydrogel's modulus in a predictable manner to probe how varying the extent of degradation impacts crypt formation and architecture. In order to identify a range of soft moduli to utilize, a hydrogel solution of 5 wt% of PEG-DBCO (10 mM DBCO) and allyl sulfide (8 mM azide) was reacted *in situ* on a shear rheometer and reached a final modulus of ~1.3 kPa +/− 300 Pa. After complete gel formation, hydrogels were removed from the rheometer and allowed to equilibrium swell for 30 minutes in a solution containing 1 mM LAP and 15 mM GSH in 100 mM MOPS buffer at 7.4 pH. To minimize side reactions, a monofunctionalized azide was introduced to cap any unreacted, pendant DBCO groups.[15] The storage modulus was monitored by shear rheology while gels were exposed to 365 nm light (5 mW cm^{-2}) for exposure times of 0 to 10 s. Degradation under these conditions yields storage modulus values from 5 to 60% of the original modulus (Figure 2b), where a post-degradation shear storage of ~600 Pa has been identified as ideal for in situ crypt formation from intestinal organoids.[6] Degradation was further characterized through swelling studies, in which the mass of hydrogels were compared before and after softening. No significant differences were seen in degree of swelling between all five soft conditions, likely due to these hydrogels initially existing far from their equilibrium swelling point and due to their high water content (99%) (Figure S2). Further rheological characterization revealed that the moduli of any soft condition did not depend on frequency (Figure S3). Moving forward, softening for 2, 5, 8 and 10 seconds

were selected, which correlates to softening between 5 and 60% of the original modulus (~1300 Pa) (Figure 2b).

3. Colony Survival Exhibits Moduli Dependence

Intestinal organoid maturation occurs in two phases; the first pertaining to the formation of colonies from single intestinal stem cells and the second consists of budding of ISC colonies to form crypts and differentiated cell types.[1,6] When studying crypt formation, it may be advantageous to circumvent the first colony forming step by encapsulating colonies from Matrigel into synthetic hydrogels, as it is time consuming and often yields a low number of colonies in synthetic matrices. As mentioned previously, Gjorevski *et al* proposed an ideal synthetic matrix modulus for colony growth from single intestinal stem cells.[6] However, studies to date have not investigated the survival and mechanical dependence of colonies extracted directly from Matrigel and encapsulated into synthetic matrices.

To this end, Lgr5-GFP+ intestinal stem cell colonies extracted from Matrigel were encapsulated in PEG-allyl sulfide hydrogels functionalized with RGD at 0.8 mM using the same 3–7 wt% macromer formulations used in chapter 2. Colony survival was greatest in the 5 wt% condition (1.3 kPa) (Figure 3a). Colony survival four days after encapsulation was denoted by epithelium polarization as marked by F-actin. Stem maintenance and lgr5 expression was marked by GFP expression (Figure 3b). Either a higher or lower modulus resulted in a decreased number of living colonies, thereby demonstrating the survival of intestinal organoid colonies are similarly dependent as individual ISCs on matrix moduli. Colony size and shape were further quantified, with size following a similar trend to viability and with no differences in shape between the conditions (Figure S4). Macromer weight percent influences the cross-linking density of the hydrogel, which simultaneously influences the modulus, equilibrium water content, the mesh size and diffusivity. These PEG-allyl sulfide hydrogels have an equilibrium water content of 99% water. In this range, components in the culture media and many cell secreted molecules can diffuse on a time scale of seconds to minutes, therefore it is hypothesized that the modulus and mechanosensing has a more significant effect than the pore size.[24–27] We hypothesize that lower weight percent hydrogels do not provide the compressive support needed to hold the epithelium in place.[6] Further, by observation at higher weight percent gels, colonies began to have a more elongated rather than spherical morphology (Figure 3b), implying matrix forces may be acting to create this deformation. It is possible that at these higher weight percent formulations, an increase in hydrogel swelling (upon equilibration) applies a swelling force to the encapsulated colonies, decreasing their survival.[28,29] In this case, decreased survival could also be attributed to osmotic effects.[30,31] While Matrigel might seem to contradict these hypotheses as it is a very soft material, Matrigel and other protein materials have been shown to exhibit strain stiffening behavior, meaning organoids would experience higher local forces.[32–34]

4. Crypt Architecture is Mechanosensitive

As colony survival was mechanosensitive, we were interested in investigating how crypt formation and architecture responded to mechanical cues. By controlling the duration of

light exposure, we previously demonstrated that we can precisely manipulate the hydrogel's modulus in a predictable manner to probe how varying the extent of degradation impacts crypt formation and architecture. In order to ensure that the degradation conditions did not affect colony survival, we encapsulated intestinal stem cell colonies harvested from Matrigel into the same 5 wt% hydrogels. After 24 hours in growth media, the hydrogels were equilibrated with 1 mM LAP and 15 mM GSH in Flurobrite media. The hydrogels were then irradiated for 0–10 seconds and immediately switched to differentiation media. At two days post softening, organoids were fixed and analyzed for survival, based on epithelial polarization. Softening under 10 seconds showed no significant change to the colony polarization (Figure 4a). Additionally, intestinal organoids showed no differences in viability when exposed to 0–10 seconds of UV light without LAP or GSH (Figure S5). At three days post softening, colonies were fixed and immunostained for lysozyme, a marker of Paneth cells which are known to reside in the crypt (Figure 4b).[6]

Encapsulated colonies were imaged on a two-photon laser scanning confocal microscope and analyzed for crypt forming efficiency, which we define as the number of living colonies that form crypts. Crypt forming efficiency was highest for 5 seconds of degradation, or when 15% of the matrix is softened. Softening for greater or less than 5 seconds resulted in decreases in crypt forming efficiency, with no crypts forming in the control (0 second) condition. This trend demonstrates that the ability of a colony to form crypts is dependent on their local matrix stiffness while differentiating (Figure 4c).

As crypt formation was dependent on the extent of matrix softening, we next examined the resulting crypt architecture as a function of degradation. Crypt architecture was determined by investigating the crypt length at each of the conditions, as the crypt villus structure is the functional component of the intestine. A marked difference in crypt length and size is seen between species and between healthy and diseased conditions, such as celiac's disease, etc. [35,36] Crypts were identified by the presence of Paneth cells and the crypt length was measured in image editing software (ImageJ) as the longest length from the main colony body to the tip of the crypt (Figure 4d). Crypt length followed a similar trend to crypt forming efficiency, except with a maximum length occurring at 8 seconds, with an average length of 120 +/− 50 μm. Degradation lasting longer or shorter than 8 seconds demonstrated decreased crypt length, with 2 and 10 second conditions demonstrating crypts an average of 20 +/− 4 μm and 20 +/− 6 μm in length (Figure 4e). To ensure that the length of the crypt irradiated for 8 seconds was not just a factor of initial colony size, crypt length was normalized to colony diameter (longest), and still showed a similar trend (Figure S6). Thus, this variation in length is more likely a result of the matrix mechanics and not a consequence of colony size. Organoids were next analyzed for number of crypts per colony, which is of great importance in clinical applications for reproducibility purposes. A similar trend was seen with number of crypts as with crypt length, in which 8 seconds of degradation showed the greatest number of crypts per colony (3). Meanwhile, irradiation for 2 and 10 seconds maintained 1 crypt per organoid (Figure 4f). This implies that initial intestinal organoid differentiation and crypt development can be directed by bulk mechanical properties.

While organoids were immunostained with lysozyme to identify the location of crypts (Figure 4g), to ensure the development of mature crypts, organoids were immunostained for

the presence of mature cell types found in the native intestine.[3,37] Organoids formed in these photodegradable hydrogels showed the presence goblet cells (with Mucin 2), enterocytes (with L-FABP) and enteroendocrine cells (with chromogranin A). Crypts formed in all four softened conditions maintained these cells types (Figure 5).

5. Conclusion

Utilization of organoid technologies in clinical and translational applications is limited by the inability of current culture platforms to generate uniform and reproducible structures. The heterogeneity of organoid architectures stems not only from the lack of understanding of organoid developmental pathways, but also from lack of appropriate controllable materials. In this work, we report a photodegradable hydrogel platform to study the influence of matrix mechanical properties on intestinal organoid differentiation; a knowledge of which can instruct controlled crypt formation for clinical and other applications, such as drug screening. The stiffness of allyl sulfide photodegradable hydrogels was tuned by varying the extent of degradation, allowing for *in situ* control over the hydrogel mechanical environment. ISC colonies were encapsulated into allyl sulfide hydrogels, and the survival was shown to be stiffness dependent, indicating mechanosensitivity. Further, we utilized controlled photodegradation to facilitate intestinal organoid differentiation through the formation of intestinal crypts. The size and number of formed intestinal crypts was found to be dependent on the extent of matrix softening. The use of this platform can provide more uniform and consistent organoid structures. Such advances would be particularly useful in the field of drug screening, where homogenous organoid cultures may be necessary for reproducible results.

Further, this work motivates the study of mechanosensitive pathways that may be involved in colony survival and maturation. We demonstrate that these phenomena are mechanosensitive, and it has been shown that YAP/Notch signaling are key players in colony formation and crypt maintenance.[38,39] Therefore, it would be of interest to compare YAP/Notch signaling in different mechanical environments to better understand organoid dependence on local matrix mechanics. This information would further instruct platforms for producing uniform crypts. Altogether, this work introduces the mechanical dependence of crypt architecture and will serve to guide future studies into uniform, crypt structure.

6. Experimental Section

PEG Precursor Synthesis

Four arm, 20 kDa PEG-dibenzylcyclooctyne (PEG-4DBCO) macromers were synthesized by coupling DBCO-C6 acid (1 equiv, MW=20,000, JenKem USA) using 1-[Bis(dimethylamino)methylene]-1H-1,2,3-triazolo[4,5-b]pyridinium 3-oxidhexafluorophosphate (HATU, ChemPep, 1.5 equiv) as an activator and 4 methyl-morpholine as a base (4 equiv, Alfa Aesar). The reaction was allowed to proceed overnight, after which the mixture was precipitated in cold ether to yield an off white solid. The product was collected by centrifugation, dissolved in water, dialyzed for 48 hours against DI water, and lyophilized to yield the final product (69.7% yield, 99% functionalization).

Synthesis of allyl sulfide bis(azide)

The synthesis of allyl sulfide bis(azide) was carried out at previously described.[14]

Rheological Characterization of SPAAC Hydrogel Polymerization

Stock solutions of hydrogel precursors were prepared as 20 wt% PEG-4DBCO in phosphate buffered saline (PBS) and 50 mM allyl sulfide crosslinkers in DMSO. Hydrogels containing allyl sulfide crosslinks were formed by strain promoted azide-alkyne cycloaddition (SPAAC) by mixing stock solutions with PBS to a final concentration of 3–7 wt% PEG-4DBCO and 5 mM allyl sulfide crosslinker in PBS. After mixing, the precursor solutions were vortexed for 10 seconds and placed as 20 μL drops between two glass, Sigmacoted slides separated with 0.5mm rubber spaces. The glass slides were clamped together with paper clips and allowed to polymerize for >15 min. The samples were then transferred to a TA instruments' DHR-3 rheometer with an 8mm parallel plate geometry. Oscillation fast sampling rheometery was performed with 5% strain and a frequency of 1.0 Hz.

Rheological Characterization of SPAAC Hydrogel Degradation

Hydrogel precursor solutions and hydrogels were formed as described previously. After polymerizing for >15 min, hydrogels were equilibrated in 100 mM MOPS buffers at pH 7.4, 1 mM LAP and 15 mM glutathione for 30 minutes. Oscillation rheology was then performed with an 8 mm parallel plate geometry on a TA instruments DHR-3 rheometer. The rheometer was fitted with an adaptor to allow for light exposure from a mercury arc lamp (Omnicure) fitted with a 365 nm bandpass filter. Storage and loss moduli were recorded using a strain of 5 % and 1 Hz while samples were irradiated with 365 nm light at 5 mW cm^{-2} for 0 to 10 seconds.

Crypt Isolation and Organoid Culture

Murine small intestinal crypts were isolated from Lgr5-eGFP-IRES-CreERT2 mice as previously described.[37] The crypts were maintained as organoids by encapsulation in reduced growth factor Matrigel (Corning). The organoids were cultured in growth media, composed of Advanced DMEM-F12 (Invitrogen) with N2 and B27 supplements (Thermo Fischer Scientific), Glutamax (Gibco), HEPES, penicillin-streptomycin, and supplemented with epidermal growth factor (50 ng mL^{-1}, R&D Systems), Noggin (100 ng mL^{-1}, PeproTech), R-Spondin conditioned media (5% v/v), CHIR99021 (3 μM, Selleckchem), valproic acid (1 mM, Sigma-Aldrich) and n-acetylcysteine (1 μM, SigmaAldrich). The medium was changed every 2 days, and organoids were released from Matrigel, sheared and resuspended in Matrigel every 4 days.

Encapsulation of Colonies into Photodegradable Gels

24 hours prior to encapsulation, organoids were released from Matrigel, sheared and resuspended in Matrigel. Hydrogel precursor solutions were prepared by diluting 4-arm PEG-DBCO in Advanced DMEM-F12 media supplemented with Glutamax, HEPES, and penicillin-streptomycin to varying concentrations. Azide functionalized RGD (0.8 mM) was added to the hydrogel precursor solutions, which were kept on ice until the addition of cells. The organoids were then released from Matrigel using cold DMEM-F12 followed by

mechanical stimulations. The organoid suspension was then centrifuged (1200 RPM, 4 minutes) and the resulting pelleted was resuspended in DMEM-F12 media. 8 μL of mouse derived laminin (Gibco) was added to hydrogel precursors, followed by the cell suspension. Gelation was initiated by the addition of allyl sulfide bis(azide), such that the allyl sulfide azide groups were on stoichiometry with total DBCO groups. The solution was vortexed for 5 seconds and 20 μL drops were placed on thiolated coverslips. After 15 minutes, DMEM-F12 plus the appropriate growth media supplements were added.

Quantification of Living Colonies

Colonies growing in allyl sulfide hydrogels were fixed with 4% paraformaldehyde (30 min, room temperature) following 4 days of growth. A laser scanning confocal microscope (Zeiss LSM 710) with a 488 nm laser was used to collect z-stack images of organoids spanning the thickness of the gel. ImageJ (NIH) was used to investigate the GFP expression of Lgr5+ cells to ensure colonies maintained stemness. Fixed colonies were also immunostained for F-actin and DAPI. After fixation, ISC colonies were solubilized using 0.2% Triton X-100 (Sigma) in PBS (1 hour at room temperature) and blocked using 10% goat serum (Gibco) and 0.01% Triton X-100 in PBS (overnight, 4°C). The samples were incubated with rhodamine phalloidin (1 U mL^{-1}, Invitrogen) and DAPI (1.5μM) in blocking buffer. After washing with PBS four times to remove any residual antibody, the fluorescently labeled colonies were imaged using confocal microscopy (Zeiss LSM 710). ImageJ (NIH) was used to visualize and quantify polarized colonies.

Degradation of Cell Laden Hydrogels

24 hours after encapsulation, culture media was replaced with 500 μL of Fluorobrite medium (Thermo Fischer Scientific), supplemented with N2 and B27 supplements (Thermo Fischer Scientific), 15 mM reduced glutathione (Sigma) and 1 mM LAP. The cell laden hydrogels were allowed to equilibrate for 30 minutes at 37°C, after which the hydrogels were irradiated with 365 nm light at 5 mW cm^{-2} for 0–10 seconds. After irradiation, Fluorobrite media was replaced with differentiation media, composed of Advanced DMEM-F12 (Invitrogen) with N2 and B27 supplements (Thermo Fischer Scientific), Glutamax (Gibco), HEPES, penicillin-streptomycin, and supplemented with epidermal growth factor (50 ng mL^{-1}, R&D Systems), Noggin (100 ng mL^{-1}, PeproTech), R-Spondin conditioned media (5% v/v), and n-acetylcysteine (1μM, SigmaAldrich).

Immunofluorescence Analysis

Colonies growing in softened allyl sulfide hydrogels were fixed with 4% paraformaldehyde (30 min, room temperature) 48 hours after softening. A laser scanning confocal microscope (Zeiss LSM 710) was used to collect z-stack images of organoids spanning the thickness of the gel. After fixation, ISC colonies were solubilized using 0.2% Triton X-100 (Sigma) in PBS (1 hour at room temperature) and blocked using 10% goat serum (Gibco) and 0.01% Triton X-100 in PBS (overnight, 4°C). The samples were then incubated overnight at 4°C with a rabbit primary antibody against lysozyme (1:50, Invitrogen PA1–29680) diluted in blocking buffer. The samples were then washed fresh with PBS every hour for 5 hours to remove residual primary antibody. Next, the samples were incubated with rhodamine phalloidin (1 U mL^{-1}, Invitrogen) and DAPI (1.5 μM) in blocking buffer. After washing with

PBS four times to remove any residual antibody, the fluorescently labeled colonies were imaged using confocal microscopy (Zeiss LSM 710). ImageJ (NIH) was used to visualize colonies and measure crypt length.

Statistics

All data was collected using 3 hydrogel replicates per condition, with the exception of figure 4, which was conducted with 4 hydrogel replicates per condition. For each gel, at least 15 organoids were analyzed, except for gels degraded for 10 seconds, which have at least 10 organoids analyzed per gel. Data was compared using one-way ANOVA and Tukey posttests or Student's *t*-test in Prism 8 (GraphPad Software, Inc). Data are presented as means ± standard deviation.

Supplementary Material

Refer to Web version on PubMed Central for supplementary material.

Acknowledgements

We thank the Lutolf group at EPFL for generously providing our group with intestinal stem cells. We would also like to thank Mark W. Young for help with intestinal organoid passaging. This work was funded by the NIH R01 DK120921. E.A.H and F.M.Y acknowledge the DoE GAANN fellowship for funding. T.E.B was supported by the NSF GRFP. A portion of Figure 4a was created with BioRender.com.

References

[1]. Sato T, Vries RG, Snippert HJ, van de Wetering M, Barker N, Stange DE, van Es JH, Abo A, Kujala P, Peters PJ, et al., Nature 2009, 459, 262. [PubMed: 19329995]

[2]. Serra D, Mayr U, Boni A, Lukonin I, Rempfler M, Challet Meylan L, Stadler MB, Strnad P, Papasaikas P, Vischi D, et al., Nature 2019, 569, 66. [PubMed: 31019299]

[3]. Kong S, Zhang YH, Zhang W, Biomed Res. Int. 2018, 2018, DOI 10.1155/2018/2819154.

[4]. Barker N, Nat. Rev. Mol. Cell Biol. 2014, 15, 19. [PubMed: 24326621]

[5]. Cruz-Acuña R, Quirós M, Farkas AE, Dedhia PH, Huang S, Siuda D, García-Hernández V, Miller AJ, Spence JR, Nusrat A, et al., Nat. Cell Biol. 2017, 19, 1326. [PubMed: 29058719]

[6]. Gjorevski N, Sachs N, Manfrin A, Giger S, Bragina ME, Ordóñez-Morán P, Clevers H, Lutolf MP, Nature 2016, DOI 10.1038/nature20168.

[7]. Arakawa CK, Badeau BA, Zheng Y, DeForest CA, Adv. Mater. 2017, 29, 1703156.

[8]. Uto K, Tsui JH, DeForest CA, Kim D-H, Prog. Polym. Sci. 2017, 65, 53. [PubMed: 28522885]

[9]. DeForest CA, Polizzotti BD, Anseth KS, Nat. Mater. 2009, 8, 659. [PubMed: 19543279]

[10]. Agard Nicholas J., and Prescher Jennifer A., Bertozzi CR*, 2004, DOI 10.1021/JA044996F.

[11]. Griffin DR, Kasko AM, J. Am. Chem. Soc. 2012, 134, 13103. [PubMed: 22765384]

[12]. Ifkovits JL, Burdick JA, Tissue Eng. 2007, 13, 2369. [PubMed: 17658993]

[13]. Madl CM, Katz LM, Heilshorn SC, Adv. Funct. Mater. 2016, 26, 3612. [PubMed: 27642274]

[14]. Brown TE, Marozas IA, Anseth KS, Adv. Mater. 2017, 29, 1605001.

[15]. Brown TE, Silver JS, Worrell BT, Marozas IA, Yavitt FM, Günay KA, Bowman CN, Anseth KS, J. Am. Chem. Soc. 2018, 140, 11585. [PubMed: 30183266]

[16]. Killaars AR, Grim JC, Walker CJ, Hushka EA, Brown TE, Anseth KS, Adv. Sci. 2019, 6, 1801483.

[17]. Grim JC, Brown TE, Aguado BA, Chapnick DA, Viert AL, Liu X, Anseth KS, 2018, DOI 10.1021/acscentsci.8b00325.

[18]. Smet M, Liao L-X, Dehaen W, McGrath DV, Org. Lett. 2000, 2, 511. [PubMed: 10814364]

[19]. Kevwitch RM, McGrath DV, New J Chem. 2007, 31, 1332.
[20]. Kim MS, Diamond SL, Bioorg. Med. Chem. Lett. 2006, 16, 4007. [PubMed: 16713258]
[21]. Kloxin AM, Kasko AM, Salinas CN, Anseth KS, Science 2009, 324, 59. [PubMed: 19342581]
[22]. Kharkar PM, Kiick KL, Kloxin AM, Chem. Soc. Rev. 2013, 42, 7335. [PubMed: 23609001]
[23]. Hodgson SM, Bakaic E, Stewart SA, Hoare T, Adronov A, Biomacromolecules 2016, 17, 1093. [PubMed: 26842783]
[24]. Rehmann MS, Skeens KM, Kharkar PM, Ford EM, Maverakis E, Lee KH, Kloxin AM, Biomacromolecules 2017, 18, 3131. [PubMed: 28850788]
[25]. Lee S, Tong X, Yang F, Acta Biomater. 2014, 10, 4167. [PubMed: 24887284]
[26]. Salgado AJ, Coutinho OP, Reis RL, Macromol. Biosci. 2004, 4, 743. [PubMed: 15468269]
[27]. El-Sherbiny IM, Yacoub MH, Glob. Cardiol. Sci. Pract. 2013, 2013, 316. [PubMed: 24689032]
[28]. S. R. Caliari, J. A. Burdick, Nat. Methods 2016, 13, 405. [PubMed: 27123816]
[29]. Perera D, Medini M, Seethamraju D, Falkowski R, White K, Olabisi RM, Microencapsul J. 2018, 35, 475.
[30]. Gonzalez-Pujana A, Rementeria A, Blanco FJ, Igartua M, Pedraz JL, Santos-Vizcaino E, Hernandez RM, Drug Deliv. 2017, 24, 1654. [PubMed: 29078721]
[31]. Carvalho AF, Gasperini L, Ribeiro RS, Marques AP, R. l. Reis, J. Tissue Eng. Regen. Med. 2018, 12, e1063. [PubMed: 28342296]
[32]. Rudnicki MS, Cirka HA, Aghvami M, Sander EA, Wen Q, Billiar KL, Biophys. J. 2013, 105, 11. [PubMed: 23823219]
[33]. Storm C, Pastore JJ, MacKintosh FC, Lubensky TC, Janmey PA, Nature 2005, 435, 191. [PubMed: 15889088]
[34]. Jaspers M, Dennison M, Mabesoone MFJ, MacKintosh FC, Rowan AE, Kouwer PHJ, Nat. Commun. 2014, 5, DOI 10.1038/ncomms6808.
[35]. Kellett M, Potten CS, Rew DA, Epithelial Cell Biol. 1992, 1, 147. [PubMed: 1307946]
[36]. Dickson BC, Streutker CJ, Chetty R, J. Clin. Pathol. 2006, 59, 1008. [PubMed: 17021129]
[37]. Gjorevski N, Sachs N, Manfrin A, Giger S, Bragina ME, Ordóñez-Morán P, Clevers H, Lutolf MP, Nature 2016, DOI 10.1038/nature20168.
[38]. Azzolin L, Panciera T, Soligo S, Enzo E, Bicciato S, Dupont S, Bresolin S, Frasson C, Basso G, Guzzardo V, et al., Cell 2014, 158, 157. [PubMed: 24976009]
[39]. Totaro A, Castellan M, Battilana G, Zanconato F, Azzolin L, Giulitti S, Cordenonsi M, Piccolo S, Nat. Commun. 2017, 8, 15206. [PubMed: 28513598]

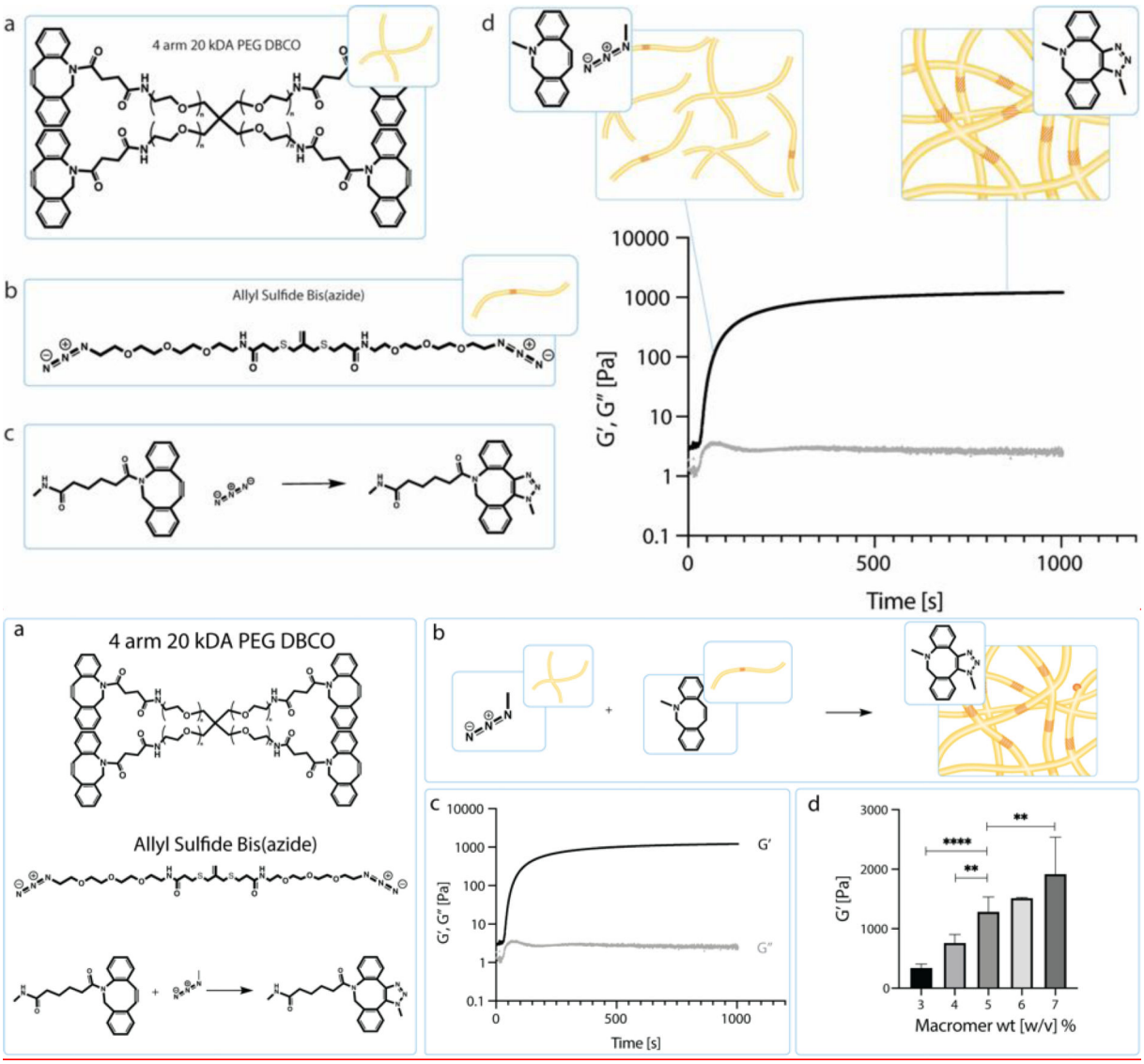

Figure 1.

a) Schematic of the chemical structure of 4 arm 20 kDa PEG DBCO and the chemical structure of allyl sulfide bis(azide). Upon mixing the PEG DBCO with the allyl sulfide bis(azide), the strained octyne will react with the azide group through a strain-promoted azide alkyne cycloaddition (SPAAC). b) Through this SPAAC formation, a hydrogel network is formed. The red cross hatch region of the network is the photodegradable region. c) Shear storage modulus (black) and loss modulus (gray) were measured over time as the network polymerizes. Polymerization is rapid and occurs in under 5 min. d) Hydrogel moduli increase with increasing macromer wt%. Data is represented as means +/− standard deviation. An n of 3 was used and analyzed using a one-way Anova with multiple comparisons. **p<0.01, ****p<0.0001

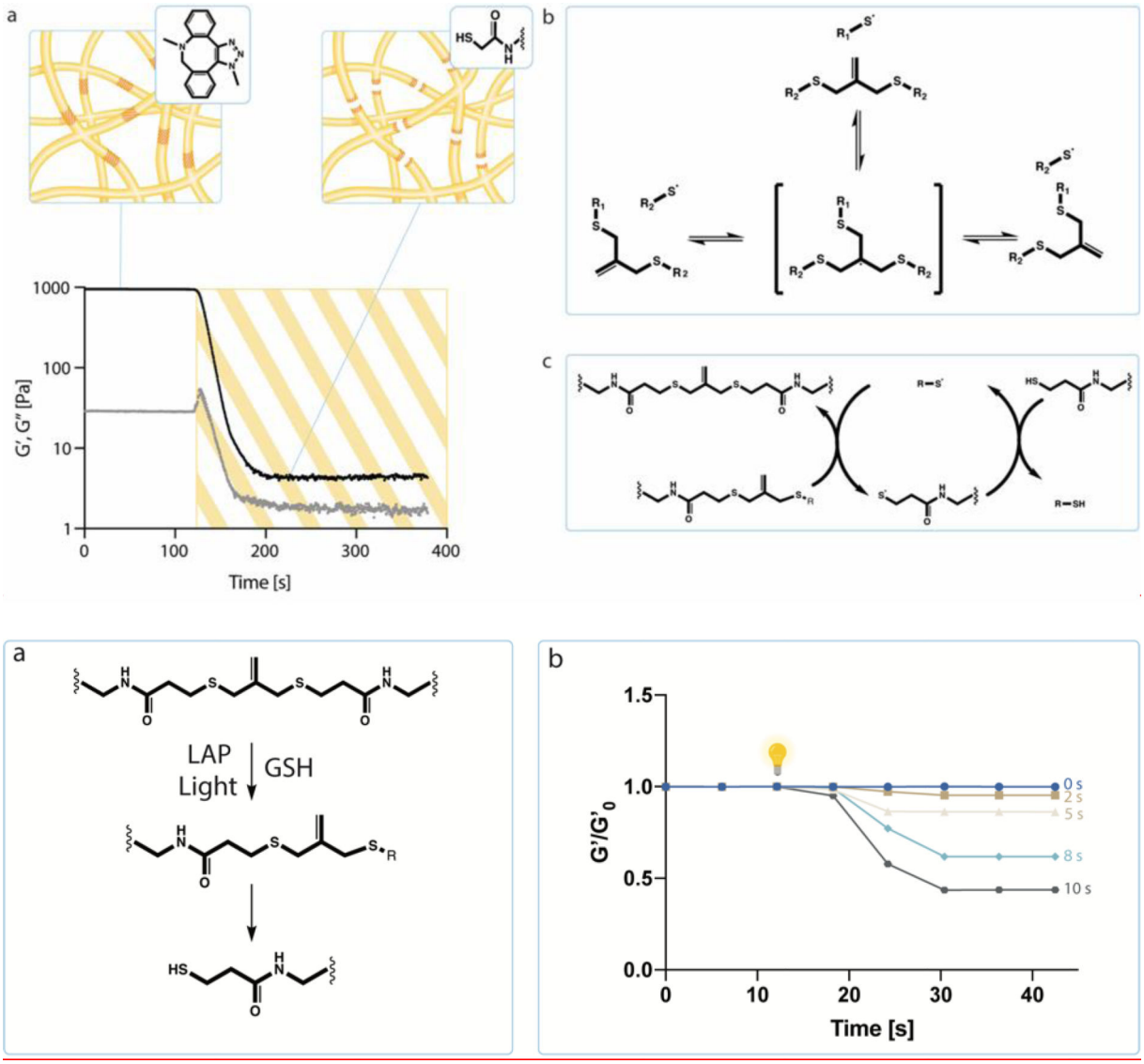

Figure 2.

a) Hydrogel network degradation initiated by free radicals. Allyl sulfide bis(azide) reacts with thiyl radicals to form a radical intermediate that undergoes beta scission. This results in the fragmentation of crosslinks and the regeneration of the thiyl radical and allyl sulfide bis(azide). A soluble thiol species (glutathione) exchanges with the allyl sulfide bis(azide), therefore producing a cleaved crosslink and a network tethered thiyl radical. The released network thiyl radical undergoes chain transfer to a soluble thiol species, which can initiate further exchanges, creating an amplified degradation process. b) Hydrogels that were swollen with glutathione and LAP were irradiated with 365 nm light, creating a range of soft conditions that varied from around 500 Pa to 1.3 kPa.

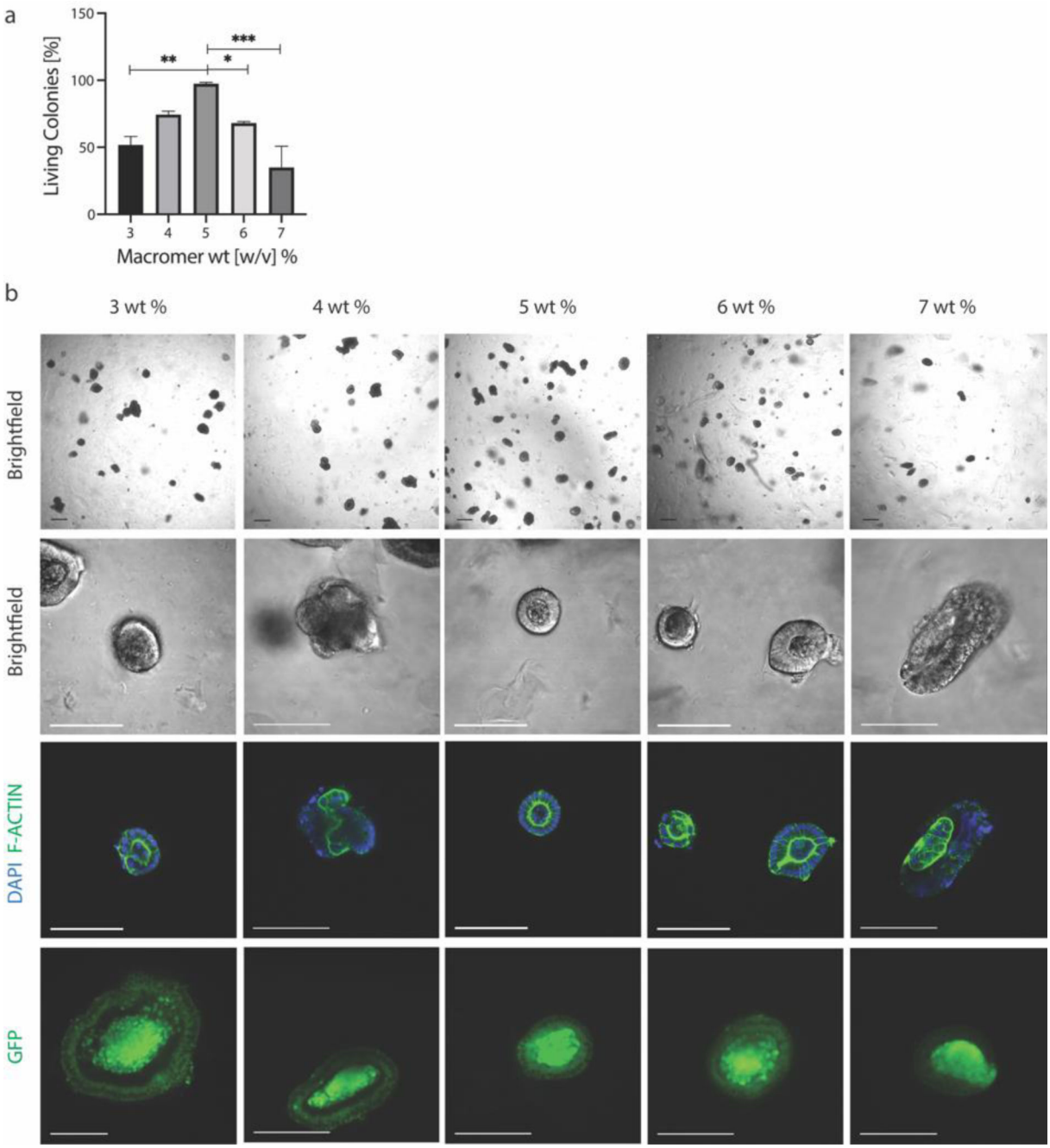

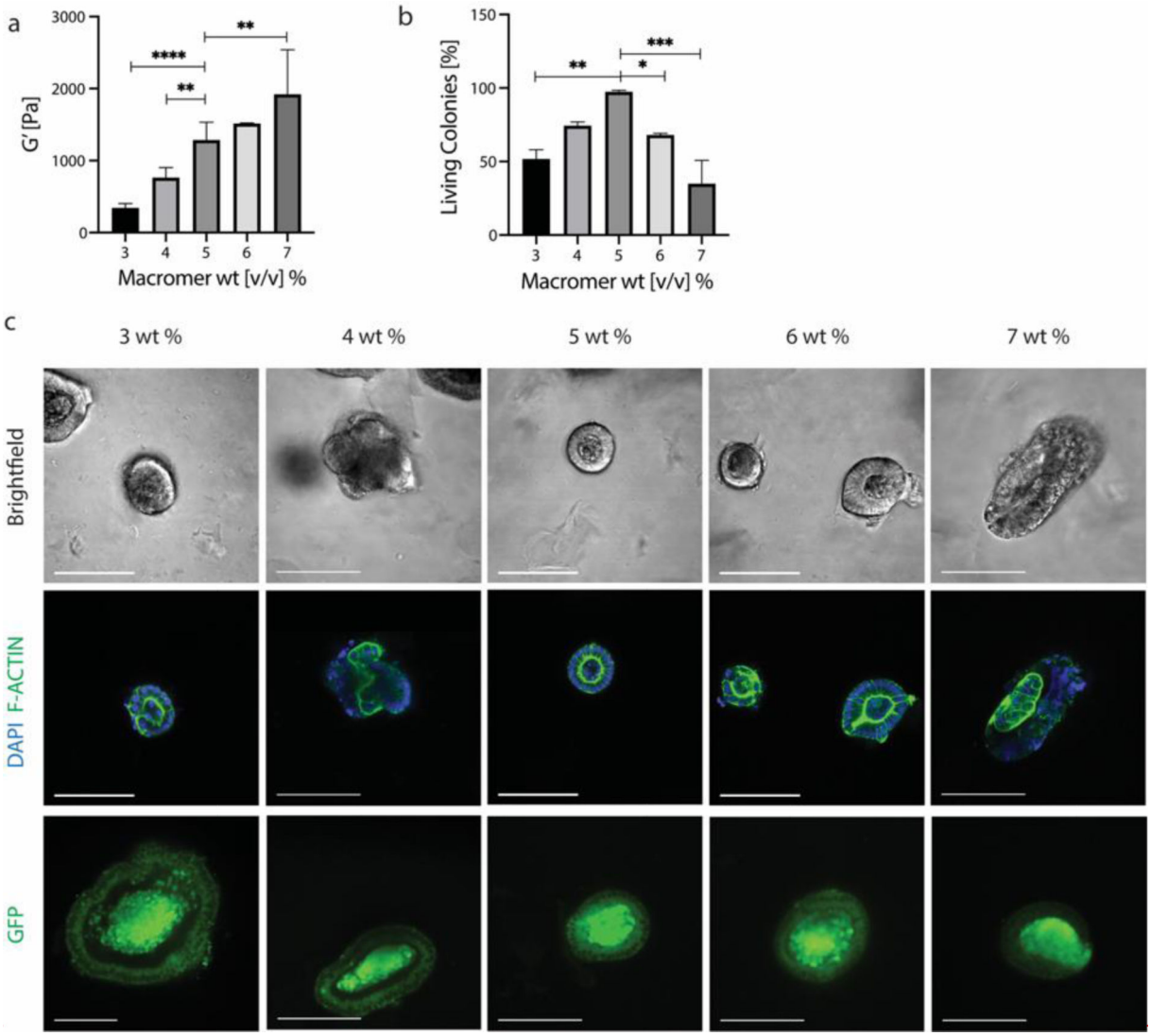

Figure 3.

a) ISC colony survival is dependent on macromer wt%, and therefore modulus, with the highest viability seen at 5 wt% and 1.3 kPa. b) ISC colonies were marked as viable if they maintained stemness, as marked by GFP expression, and were polarized, as visualized by F-Actin staining. Scale bar 100 μm. Data is represented as means +/− standard deviation. At least three hydrogels were analyzed per condition and data was analyzed using a one-way Anova with multiple comparisons. *$p<0.05$, **$p<0.01$, ***$p<0.001$

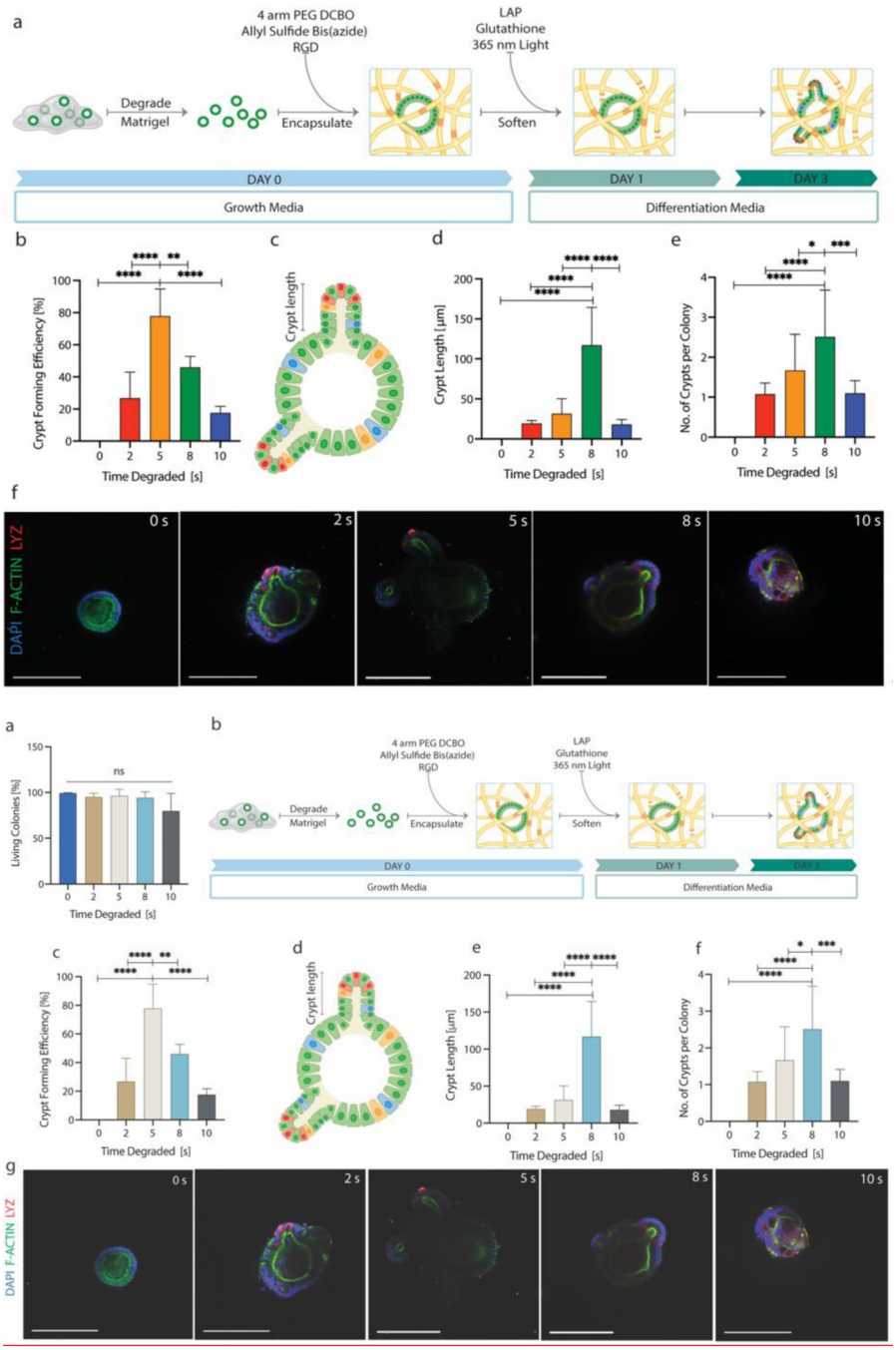

Figure 4.

a) When encapsulated in hydrogels that were subsequently softened, colony viability was maintained and unaffected by irradiation for less than 10 seconds of exposure. b) To study crypt formation as a function of hydrogel moduli, ISC colonies were released from Matrigel and encapsulated in photodegradable hydrogels. After 24 hours, hydrogels were swollen with LAP and Glutathione in Flurobrite media for 30 minutes and then irradiated with 365 nm light. After irradiation, colonies were switched to differentiation media. 48 hours after softening, colonies were fixed and immunostained. c) Cell laden hydrogels were softened for

0, 2, 5, 8 or 10 seconds and crypt forming efficiency was quantified as the percentage of living colonies that formed crypts. d) Resulting crypts were measured by quantifying the distance from the main colony body to the tip of the crypt. e) Crypt length was quantified for all softening conditions and showed moduli dependence, f) as did the number of crypts that formed per colony. g) Crypts were marked by the presence of lysozyme producing Paneth cells. Scale bar 100 μm. Data is represented as means +/− standard deviation. At least three hydrogels were analyzed per condition and data was compared using a one-way Anova with multiple comparisons. *$p<0.05$, **$p<0.01$, ***$p<0.001$, ****$p<0.0001$

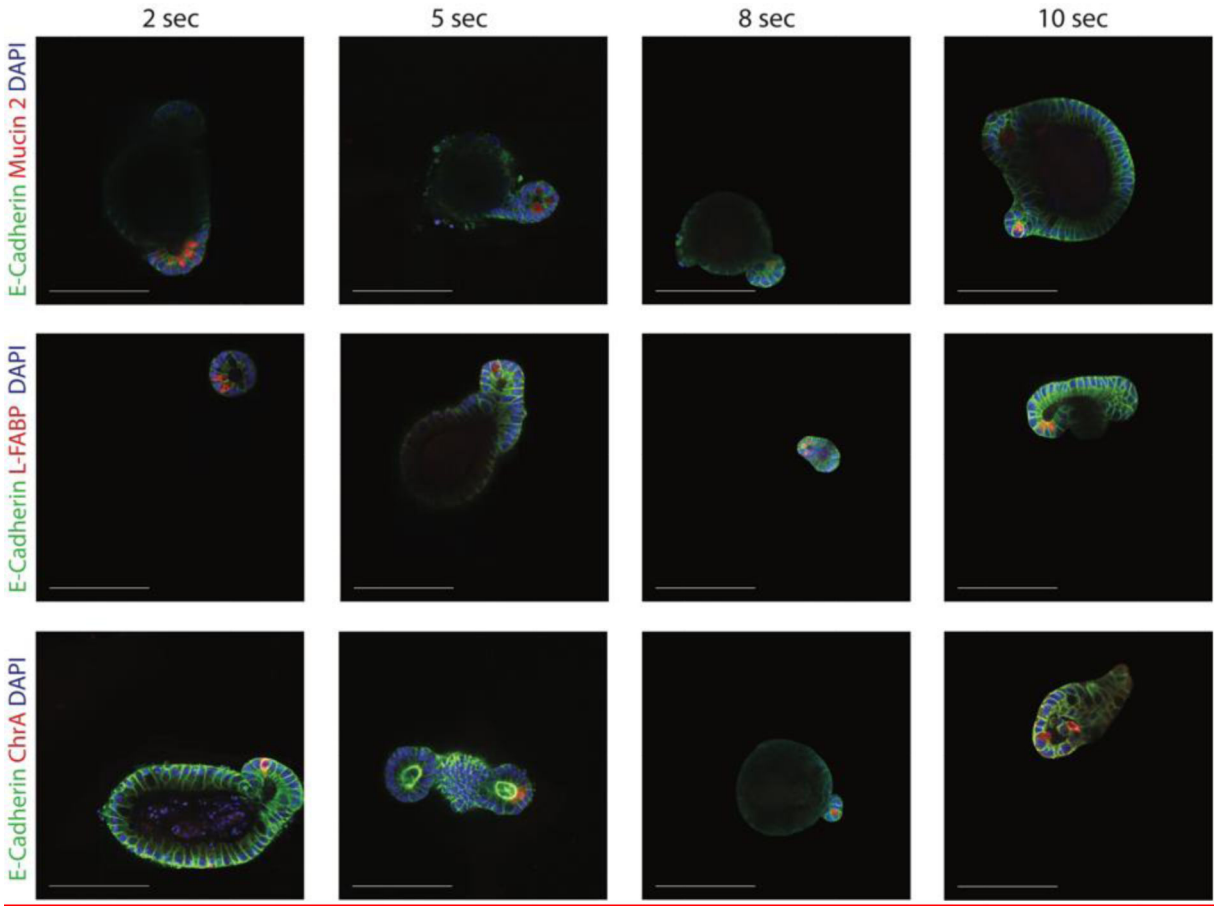

Figure 5.

Organoids produced in all four soft hydrogel conditions were immunostained for the presence of differentiated cell types commonly found in the native intestine. Specifically, organoids were immunostained for E-cadherin, goblet cells (mucin 2), enterocytes (L-FABP) and enteroendocrine cells (Chromogranin A).